applied sciences

MDPI

Article

Indolocarbazole-Based Hosts for Efficient Red Phosphorescent OLEDs

Mahendra Godi †, Changjun Lee †, Changmin Lee, Sangwook Park, Saeyoung Oh, Kiho Lee, Hayoon Lee and Jongwook Park *

Integrated Engineering, Department of Chemical Engineering, Kyung Hee University, Yongin-si 17104, Gyeonggi-do, Republic of Korea; mhdr0824@khu.ac.kr (M.G.); changjun.lee@khu.ac.kr (C.L.); lchm1107@khu.ac.kr (C.L.); pswook@khu.ac.kr (S.P.); tpdud5821@khu.ac.kr (S.O.); kiholee@khu.ac.kr (K.L.); kssarang1@khu.ac.kr (H.L.)

* Correspondence: jongpark@khu.ac.kr; Tel.: +82-31-201-3675

† These authors contributed equally to this work.

Abstract

Two indolocarbazole-based host materials, namely, 5,7-di([1,1′:3′,1″-terphenyl]-5′-yl)-3,9-di-tert-butyl-5,7-dihydroindolo[2,3-b]carbazole (InCz-TP) and 4,4′-(3,9-di-tert-butylindolo[2,3-b]carbazole-5,7-diyl)bis(N,N-diphenylaniline) (InCz-TPA), were designed and synthesized for application in red phosphorescent organic light-emitting diodes (OLEDs). In these systems, bulky substituents possessing tailored electron-donating characteristics were incorporated into the indolocarbazole core. The triplet energy levels were experimentally determined to be 2.81 eV and 2.78 eV, indicating that both materials are appropriate host candidates for red phosphorescent OLEDs. Device evaluations revealed that InCz-TPA delivered superior performance compared to InCz-TP, reaching a maximum external quantum efficiency (EQE) of 8.50%, which corresponds to a 36% enhancement. Both devices exhibited an electroluminescence peak at 628 nm along with nearly identical CIE coordinates of (0.678, 0.317) and (0.680, 0.318), suggesting efficient energy transfer between host and dopant.

Keywords: OLED; host; red phosphorescence; indolocarbazole

1. Introduction

Phosphorescent emitters utilize triplet excitons through the heavy atom effect, enabling a theoretical internal quantum efficiency (IQE) of up to 100%. This characteristic has driven their extensive adoption in organic light-emitting diode (OLED) emitting layers [1]. However, an increase in dopant concentration commonly leads to a decline in device efficiency, which can be attributed to aggregation-caused quenching, triplet–triplet annihilation, and triplet–polaron annihilation [2–4].

Accordingly, the host material employed with the dopant plays a decisive role, and several essential criteria must be fulfilled. First, the host should possess a higher triplet energy level (T_1) than the dopant to facilitate efficient energy transfer [5,6]. Second, a sufficiently wide band gap is required to suppress exciton confinement and trap formation, ensuring that the highest occupied molecular orbital (HOMO) and lowest unoccupied molecular orbital (LUMO) levels of the host appropriately bracket those of the dopant [7]. Third, robust thermal stability is necessary to guarantee reliable device operation [8]. To satisfy these requirements, considerable efforts have been devoted to the development of host materials for red phosphorescent OLEDs. For instance, C.-H. Chang

Check for updates

Academic Editor: Marilou Cadatal Raduban

Received: 15 April 2026
Revised: 4 May 2026
Accepted: 6 May 2026
Published: 9 May 2026

Copyright: © 2026 by the authors. Licensee MDPI, Basel, Switzerland. This article is an open access article distributed under the terms and conditions of the Creative Commons Attribution (CC BY) license.

and Y.J. Chang reported six donor–acceptor–donor-type host systems, among which DBTS-CzP, when combined with CN-T2T in a co-host configuration and Ir(piq)$_2$acac as the emitter, achieved an external quantum efficiency (EQE) of 21.7% along with a low turn-on voltage of 2.2 V [9]. In another study, Y. Zhu and H. Meng introduced Hept-TRZ featuring an armor-like heptacyclic heteroaromatic framework; devices employing this material with Ir(dmpibq) $_2$acac reached an EQE of 29.6% and exhibited an operational lifetime (LT_{95}) of 150 h at 9590 cd/m^2 [10].

In the present work, two novel materials—5,7-di([1,1′:3′,1″-terphenyl]-5′-yl)-3,9-di-tert-butyl-5,7-dihydroindolo[2,3-b]carbazole (InCz-TP) and 4,4′-(3,9-di-tert-butylindolo[2,3-b]carbazole-5,7-diyl)bis(N,N-diphenylaniline) (InCz-TPA)—were designed and synthesized by incorporating bulky substituents with finely tuned electron-donating properties into the indolo[2,3-b]carbazole (InCz) framework. Indolocarbazole derivatives, which arise from various isomeric configurations depending on the linkage of carbazole units, enable emission tuning from blue to red via substituent modification, making them highly versatile building blocks for both host and dopant applications. Furthermore, their favorable charge-transport characteristics allow their application to extend beyond emissive layers to hole transport layer (HTL) materials [11–15]. For example, Y. Zhao and W. Su reported four blue-emitting dopants based on indolo[3,2-b]carbazole, where PI-ICZ-PI achieved a current efficiency of 3.67 cd/A and a maximum EQE of 2.64% [16]. Additionally, K. Kumar and co-workers reported a Pd(II)-catalyzed process for the synthesis of indo-lo[3,2-a]carbazole derivatives, where the reaction proceeded under neat conditions in the presence of aqueous nonmetallic oxidant TBHP, and computational analysis confirmed their strong potential as HTL materials [17]. In this study, the synthesized InCz-TP and InCz-TPA were systematically investigated in terms of their optical and thermal characteristics, and their device performances were evaluated by employing them as host materials in red phosphorescent OLEDs.

2. Materials and Methods

2.1. General Information

All reagents and solvents were used as received without any additional purification. Analytical thin-layer chromatography (TLC) was conducted using Merck 60 F254 silica gel plates, and subsequent purification was achieved by column chromatography on Merck 60 silica gel (230–400 mesh, Burlington, MA, USA). ^{1}H NMR spectra were recorded at ambient temperature in $CDCl_3$ and DMSO-d_6 using a JNM-ECZ400S/L1 spectrometer (JEOL, Tokyo, Japan). UV–visible absorption spectra were obtained with a UV-1900i UV/Vis/NIR spectrophotometer (Shimadzu, Kyoto, Japan), whereas steady-state photoluminescence (PL) measurements were carried out using a PerkinElmer LS55 spectrometer equipped with a xenon flash lamp (PerkinElmer, Inc., Waltham, MA, USA). Absolute photoluminescence quantum yields (PLQYs) were determined using a Quantaurus-QY C11347 system (Hamamatsu Photonics, Shizuoka, Japan), and fluorescence lifetimes were evaluated via time-resolved photoluminescence (TRPL) measurements performed on a Quantaurus-Tau spectrometer (Hamamatsu Photonics, Shizuoka, Japan). Low-temperature photoluminescence (LTPL) measurements were further conducted to estimate the triplet energy (T_1) using a FluoroMate FS-2 spectrophotometer (SCINCO, Seoul, Republic of Korea). Computational analysis, including natural transition orbital (NTO) calculations, was carried out with the ORCA package (version 5.0.4) at the B3LYP-D3/def2-TZVPP level of theory. Thermal properties, including the glass transition temperature (T_g) and melting temperature (T_m), were analyzed by differential scanning calorimetry (DSC) using a DSC 26 instrument (TA Instruments, New Castle, DE, USA) under a nitrogen atmosphere. Thermal decomposition temperatures (T_d) were determined by thermogravimetric analysis (TGA) using an SDT

Q600 system (TA Instruments), with samples heated to 800 °C at a rate of 10 °C/min. The HOMO energy levels were determined using ultraviolet photoelectron yield spectroscopy (Riken Keiki AC-2, Nara, Japan) at the core facility center for anal-ysis of optoelectronic materials and devices of the Korea basic science institute (KBSI). The LUMO levels were subsequently estimated from the HOMO energies and corresponding optical band gaps. Thin films were prepared via vacuum deposition of the synthesized materials to a thickness of 50 nm at a rate of 1 Å/s under a pressure of 10^{-6} torr. The same deposition conditions were applied during device fabrication to form organic layers over an active area of 4 mm^2. The device structure was completed by sequentially depositing LiF and Al without exposure to ambient conditions. A Keithley 2400 source meter (Tektronix, Cleveland, OH, USA) was employed to evaluate current density (J)–voltage (V)– luminance (L) characteristics, with luminance captured by a Minolta CS-1000A spectroradiometer (Konica Minolta, Tokyo, Japan). Finally, all fabricated devices were encapsulated and stored in a glovebox to minimize degradation caused by oxygen and moisture.

2.2. Synthesis

2.2.1. Synthesis of 1,5-Dibromo-2,4-dinitrobenzene (**1**)

To a chilled and agitated solution of concentrated sulfuric acid (6.5 mL) and fuming nitric acid (6.5 mL), 1,3-dibromobenzene (7.0 g, 29.7 mmol) was added dropwise, with the temperature maintained at 10–20 °C using an ice bath. Once the addition concluded, the mixture was heated to 50 °C and stirred for an additional 30–40 min. The resulting solution was quenched by pouring it onto crushed ice, resulting in a solid precipitate. After being gathered by filtration and rinsed repeatedly with chilled water, the crude solid was dissolved in a solvent system comprising ethanol (90 mL) and acetone (20 mL). The mixture was filtered and then allowed to stand at 0 °C to facilitate recrystallization. Finally, the obtained crystals were washed with cold ethanol to yield a bright yellow solid (6.73 g, 70%). ^{1}H NMR (400 MHz, $CDCl_3$) δ: 8.45 (s, 1H), 8.22 (s, 1H).

2.2.2. Synthesis of 4,4″-Di-tert-butyl-4′,6′-dinitro-1,1′:3′,1″-terphenyl (**2**)

A suspension of compound (**1**) (5.0 g, 15.3 mmol), 2-(4-(tert-butyl) phenyl)-4,4,5,5-tetramethyl-1,3,2-dioxaborolane (10.0 g, 38.3 mmol), and $Pd(PPh_3)_4$ (0.085 g, 0.007 mmol) in 30 mL of toluene was prepared. To this, a 2 M aqueous K_2CO_3 solution (10 mL, 20.0 mmol) was introduced, and the reaction was maintained at 100 °C for 24 h. Upon cooling to ambient temperature, the reaction was halted with water. The organic phase was isolated via extraction with ethyl acetate (EA), followed by drying over anhydrous $MgSO_4$. After concentrating the solution, the residue was purified by column chromatography (eluent: EA/n-hexane = 0.5:9.5, *v*/*v*) to afford a yellow solid (5.5 g, 83%). ^{1}H NMR (400 MHz, $CDCl_3$) δ: 8.38 (s, 1H), 7.55 (s, 1H), 7.48 (d, J = 8.0 Hz, 4H), 7.29 (d, J = 8.0 Hz, 4H), 1.34 (s, 18H).

2.2.3. Synthesis of 3,9-Di-tert-butyl-5,7-dihydroindolo[2,3-b]carbazole (InCz) (**3**)

Compound (**2**) (5.0 g, 11.6 mmol), triethylphosphite (11.5 g, 69.2 mmol), and 1,2-dichlorobenzene (1 mL) were combined and heated to 180 °C for a period of 2 days under a nitrogen atmosphere. Following cooling to room temperature, the volatiles were stripped off under vacuum. The resulting crude material was subsequently purified via ethanol-based recrystallization, providing the title compound (1.35 g, 32%) as a white solid. ^{1}H NMR (DMSO-d_6, 400 MHz) δ: 10.85 (s, 2H), 8.62 (s, 1H), 8.01 (d, J = 8.0 Hz, 2H), 7.35 (d, J = 1.5 Hz, 2H), 7.29 (s, 1H), 7.18 (d, J = 8.0 Hz, 2H), 1.35 (s, 18H) ppm; ^{13}C NMR (100 MHz, DMSO) δ: 147.77, 141.06, 140.65, 121.38, 119.30, 117.55, 116.48, 111.07,107.14, 91.22, 35.22, 32.24 ppm.

2.2.4. Synthesis of 5′-Bromo-1,1′:3′,1″-terphenyl (**4**)

In 300 mL of anhydrous toluene, 1,3,5-tribromobenzene (20.0 g, 63.5 mmol), phenyl boronic acid (18.8 g, 154 mmol), and $Pd(PPh_3)_4$ (3.75 g, 3.25 mmol) were mixed. This was followed by the addition of 100 mL of aqueous 2 M K_2CO_3. Under a nitrogen atmosphere, the mixture was refluxed at 65 °C for 12 h. Once the reaction reached completion, it was partitioned between chloroform and water. The organic fraction was subsequently dried ($MgSO_4$), filtered, and evaporated. Final purification was achieved via silica gel column chromatography using a chloroform/n-hexane mixture (1:20 *v*/*v*) to yield a white solid (12.4 g, 63%). ^{1}H NMR (400 MHz, $CDCl_3$): δ = 7.70 (s, 3H), 7.60 (d, J = 8.0 Hz, 4H), 7.44 (t, J = 8.0 Hz, 4H), 7.36 (t, J = 8.0 Hz, 2H).

2.2.5. Synthesis of 4-Bromo-N,N-diphenylaniline (**5**)

A mixture of 1,4-dibromobenzene (35.3 g, 125 mmol), diphenylamine (20.3 g, 120 mmol), 1,10-phenanthroline (2.1 g, 12 mmol), CuBr (6.5 g), and KOH (10 g) was stirred in 170 mL of *o*-xylene using a three-necked flask. The mixture was heated at reflux for 72 h under N_2 protection. After being cooled, the organic phase was separated and concentrated. The residue underwent purification by silica gel column chromatography (200–300 mesh) using petroleum ether as the mobile phase. After the solvent was removed, the product was recrystallized from ethanol, yielding white crystals (21.6 g, 63.5%). ^{1}H NMR (400 MHz, $CDCl_3$ δ): 7.33 (d, J = 8.0 Hz, 2H), 7.27–7.23 (m, 4H), 7.08–7.01 (m, 6H), 6.96 (d, J = 12.0 Hz, 2H).

2.2.6. Synthesis of 5,7-Di([1,1′:3′,1″-terphenyl]-5′-yl)-3,9-di-tert-butyl-5,7-dihydroindolo[2,3-b]carbazole (InCz-TP)

A nitrogen-purged 50 mL Schlenk flask was charged with compound (**3**) (0.35 g, 1.0 mmol), compound (**4**) (0.65 g, 2.1 mmol), $Pd_2(dba)_3$ (0.05 g, 0.06 mmol), and 20.0 mL of toluene. After 20 min of stirring at room temperature, t-BuONa (0.27 g, 3.0 mmol) and P(t-Bu)$_3$ (10% in toluene, 0.1 mmol) were added sequentially. The reaction was then conducted at 90 °C for five hours. Upon completion, the volatiles were evaporated and the crude product was purified through silica gel column chromatography (dichloromethane/n-hexane = 2:8 *v*/*v*), affording a white solid (0.62 g, 78% yield). ^{1}H NMR (400 MHz, $CDCl_3$) δ: 8.79 (s, 1H), 8.20 (d, J = 8.0 Hz, 2H), 7.85 (t, J = 4.0 Hz, 2H), 7.80 (d, J = 4.0 Hz, 4H), 7.60–7.58 (m, 8H), 7.48 (d, J = 4.0 Hz, 2H), 7.44–7.41 (m, 3H), 7.35–7.33 (m, 12H), 1.40 (s, 18H); ^{13}C NMR (101 MHz, $CDCl_3$) δ: 148.91, 143.69, 142.00, 141.72, 140.26, 139.25, 129.04, 127.91, 127.24, 125.08, 124.83, 121.85, 119.28, 118.80, 117.97, 111.18, 106.15, 89.37, 77.42, 77.31, 77.10, 76.79, 35.31, 31.94 ppm.

2.2.7. Synthesis of 4,4′-(3,9-Di-tert-butylindolo[2,3-b]carbazole-5,7-diyl)bis(N,N-diphenylaniline) (InCz-TPA)

To a 50 mL Schlenk flask containing compound (**3**) (0.35 g, 1.0 mmol), compound (**5**) (0.68 g, 2.1 mmol), and $Pd_2(dba)_3$ (0.05 g, 0.06 mmol) in 20.0 mL of toluene under nitrogen, P(t-Bu)$_3$ (10% in toluene, 0.1 mmol) and t-BuONa (0.27 g, 3.0 mmol) were added after 20 min of ambient temperature stirring. The mixture was stirred for five hours at 90 °C. After the reaction finished, the solvent was removed, and column chromatography (silica gel; EA/n-hexane = 1:9 *v*/*v*) was used to isolate a white solid (0.60 g, 73%). ^{1}H NMR (400 MHz, $CDCl_3$) δ: 8.70 (s, 1H), 8.14 (d, J = 8.0 Hz, 2H), 7.44–7.41 (m, 6H), 7.38 (d, J = 8.0 Hz, 2H), 7.32–7.21 (m, 21H), 7.07–7.06 (m, 4H), 1.40 (s, 18H); ^{13}C NMR (101 MHz, $CDCl_3$) δ: 148.68, 147.63, 146.82, 141.79, 141.63, 131.96, 129.57, 127.77, 124.94, 123.75, 123.51, 121.68, 119.12, 118.46, 117.62, 110.88, 105.99, 89.29, 77.42, 77.31, 77.11, 76.79, 35.28, 31.95 ppm.

3. Results and Discussion

3.1. Molecular Design, Synthesis and Characterization

InCz exhibits a relatively stronger electron-donating effect than carbazole and provides high PLQY, excellent thermal stability, and high charge mobility, along with structural versatility arising from its rigid framework [18–20]. However, due to its planar molecular geometry, reduced intermolecular distances in the film state can intensify π–π interactions, leading to aggregation and subsequent quenching, which lowers emission efficiency [21].

For this reason, the introduction of bulky substituents is essential when InCz is used as an emitting material. The terphenyl (TP) group effectively suppresses intermolecular packing, and its large dihedral angles between phenyl rings restrict intramolecular rotation and vibration, which led to the synthesis of InCz-TP [22,23]. In addition, triphenylamine (TPA) possesses both a bulky structure and electron-donating characteristics. Diphenylamine offers strong electron-donating ability, which can enhance emission efficiency and improve charge transport properties [24,25]. However, excessive electron-donating strength may induce intramolecular charge transfer (ICT), making it difficult to maintain blue emission and causing a shift toward the green region. Accordingly, InCz-TPA was synthesized by incorporating triphenylamine as a bulky substituent with optimized electron-donating strength.

Scheme 1 depicts the multistep synthetic pathways employed to reach the target materials. The preparation of InCz-TP and InCz-TPA involved a sequential series of chemical transformations, specifically nitration, Suzuki coupling, Cadogan cyclization, and Buchwald–Hartwig amination. Following these reactions, each product underwent purification via column chromatography. To validate the chemical identities of the synthesized compounds, extensive characterization was performed using NMR spectroscopy (Figures S1–S10).

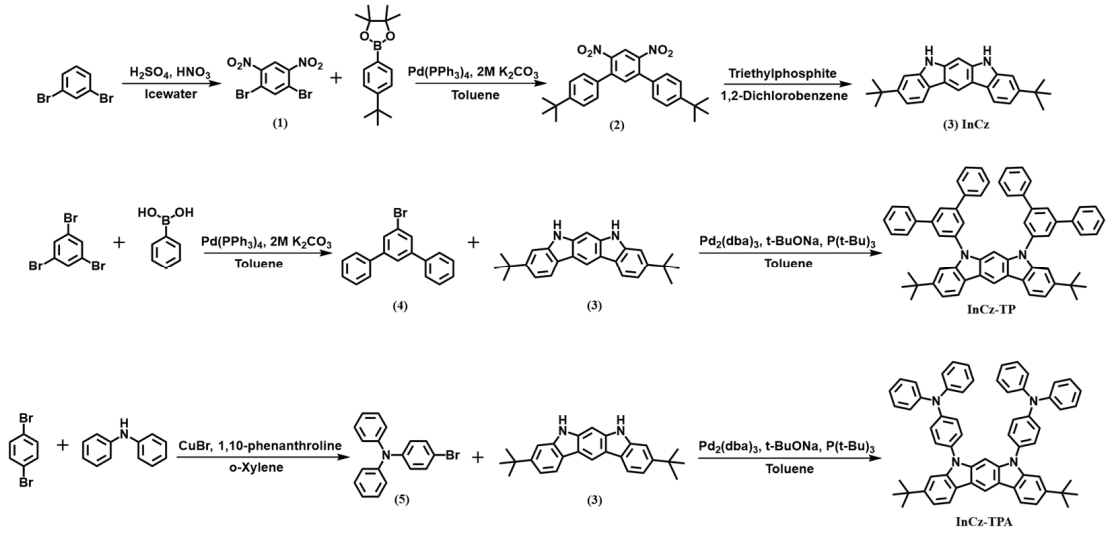

Scheme 1. Synthetic routes of the InCz-TP and InCz-TPA compounds.

3.2. Photophysical Properties

The photoluminescence (PL) and UV–vis absorption profiles of the novel emitters, InCz-TP and InCz-TPA, were recorded in toluene and as vacuum-evaporated thin films to assess their optical behavior (Figure 1). The corresponding data are compiled in Table 1. Both derivatives displayed intense absorption maxima (λ_{abs}) at approximately 310 nm across both phases, stemming from localized π–π* transitions within the aromatic framework. Furthermore, the low-intensity bands near 360 nm correspond to the delocalized n–π* transitions characteristic of the indolocarbazole core.

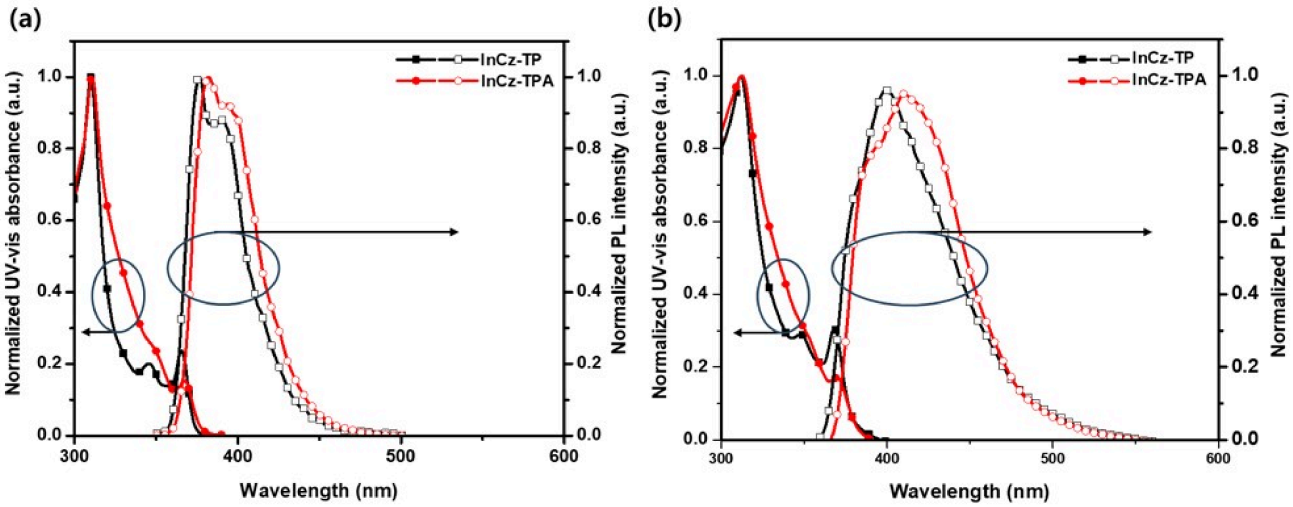

Figure 1. Normalized UV–visible absorption and PL spectra of synthesized compounds in (**a**) the solution state (toluene, 1×10^{-5} M) and (**b**) as a vacuum-deposited film (thickness: 50 nm).

Table 1. Photophysical properties of synthesized compounds.

	Solution [a]			Film [b]			PLQY [a] (%)	τ_F [a] (ns)	k_{rad} [a] (10^7 s^{-1})	k_{nr} [a] (10^7 s^{-1})
	λ_{abs} (nm)	λ_{PL} (nm)	FWHM (nm)	λ_{abs} (nm)	λ_{PL} (nm)	FWHM (nm)				
InCz-TP	310,366	376,388	38	312,369	400	69	36	4.07	8.86	15.7
InCz-TPA	311,367	382,394	41	312,370	412	72	40	3.68	10.9	16.3

[a] Toluene solution, 1.0×10^{-5} M; [b] film thickness is 50 nm.

In toluene, InCz-TP and InCz-TPA exhibited emission peaks (λ_{PL}) at 376 nm and 382 nm, respectively. The slight bathochromic shift of 6 nm observed for InCz-TPA relative to InCz-TP is likely due to the increased electron density provided by the TPA unit. Transitioning to the solid state, λ_{PL} values shifted to 400 nm for InCz-TP and 412 nm for InCz-TPA, representing red-shifts of 24 nm and 20 nm, respectively, from their solution counterparts. Such shifts toward higher wavelengths in films typically arise from enhanced molecular interactions and a denser manifold of transition states induced by shorter intermolecular spacing. Notably, the steric bulk of the TP and TPA moieties effectively moderated these shifts. The spectra broadened from solution (FWHM = 38–41 nm) to the film state (FWHM = 69–72 nm), reflecting typical solid-state aggregation effects.

The measured PLQY in solution was 40% for InCz-TPA, surpassing the 36% recorded for InCz-TP. To elucidate why InCz-TPA demonstrated superior efficiency despite the structural similarities of the TP and TPA groups, time-resolved PL (TRPL) analysis was conducted (Figure S11). The two compounds showed comparable fluorescence decay kinetics, with lifetimes (τ_F) of 4.07 ns (InCz-TP) and 3.68 ns (InCz-TPA). While the non-radiative decay rates (k_{nr}) were nearly equivalent (15.7×10^7 s^{-1} vs. 16.3×10^7 s^{-1}), InCz-TPA exhibited a notably superior radiative decay constant (k_{nr}) of 10.9×10^7 s^{-1} compared to 8.86×10^7 s^{-1} for InCz-TP. This indicates that the donating strength of the TPA group effectively promotes radiative recombination.

The electronic energy levels were determined by combining ultraviolet photoelectron yield spectroscopy for HOMO analysis with optical band gap data to calculate the LUMO positions. Absorbance edges from ($h\nu$) vs. $(\alpha h\nu)^2$ plots were utilized to identify the band gaps, where α, h, and ν represent the coefficient of absorption, Planck's constant, and photon frequency, respectively. InCz-TP possessed HOMO/LUMO energies of

−5.62 eV/−2.34 eV (E_g = 3.28 eV), alternatively, InCz-TPA showed slightly shallower levels at −5.47 eV/−2.26 eV (E_g = 3.21 eV). The tendency of the stronger TPA donor to elevate the HOMO level and contract the band gap aligns well with the red-shifted photoluminescence observed experimentally.

3.3. Theoretical Calculation

To achieve a more precise understanding of the molecular structures, geometry optimization was carried out at the B3LYP-D3/def2-TZVPP level using the ORCA computational package, as shown in Figure 2 [26]. Analysis of the dihedral angles between the InCz core and the substituent groups (TP or TPA) shows that the TP moiety in InCz-TP adopts significantly twisted conformations of 60.6° and 49.3°, which help reduce steric interactions between neighboring phenyl rings. In contrast, InCz-TPA shows comparable dihedral angles of 57.0° and 58.7°. Furthermore, NTOs of both materials were analyzed (Figure 3). In the case of InCz-TP, a significant intramolecular CT from the InCz core to the TP unit is observed. On the other hand, InCz-TPA exhibits electron density delocalized across the entire molecule because both InCz and TPA possess electron-donating characteristics, indicating a dominant locally excited (LE) state. The oscillator strength of InCz-TPA was also found to be higher than that of InCz-TP. In organic emissive molecules, the LE state generally leads to high emission efficiency due to strong orbital overlap and an increased transition dipole moment [27]. Conversely, the CT state features spatial separation between donor and acceptor regions, which reduces orbital overlap and lowers the probability of electronic transitions, resulting in comparatively lower fluorescence efficiency [28]. This interpretation agrees well with the higher PLQY experimentally measured for InCz-TPA relative to InCz-TP.

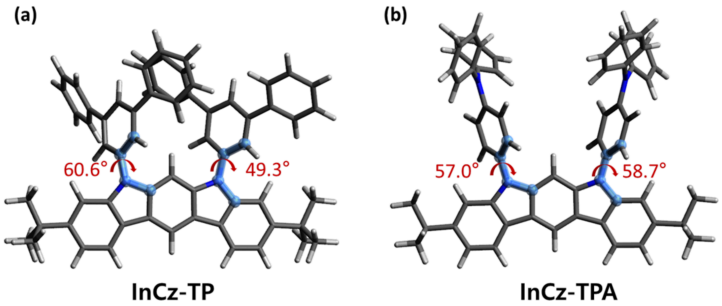

Figure 2. Optimized structures and dihedral angles calculated using B3LYP-D3/def2-TZVPP with ORCA: (**a**) InCz-TP, and (**b**) InCz-TPA.

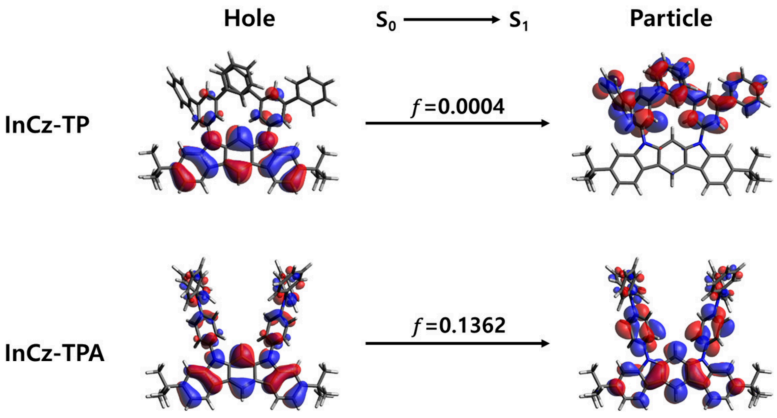

Figure 3. NTO of InCz-TP and InCz-TPA using B3LYP-D3/def2-TZVPP with ORCA.

3.4. Thermal Properties

TGA and DSC analyses were performed to investigate the thermal behavior of the synthesized host materials. According to the results illustrated in Figure 4, the decomposition temperatures (T_d), defined by a 5% mass reduction, were measured to be 440 °C for InCz-TP and 446 °C for InCz-TPA. These high thermal thresholds suggest exceptional molecular stability, which is vital for ensuring consistent OLED device performance during prolonged operation [29,30]. Regarding their phase transitions, InCz-TP and InCz-TPA exhibited T_g values of 162 °C and 140 °C, whereas T_m peaks were observed at 290 °C and 309 °C, respectively. The relatively lower melting temperature recorded for InCz-TP is likely a consequence of its comparatively weaker intermolecular interactions relative to those of InCz-TPA.

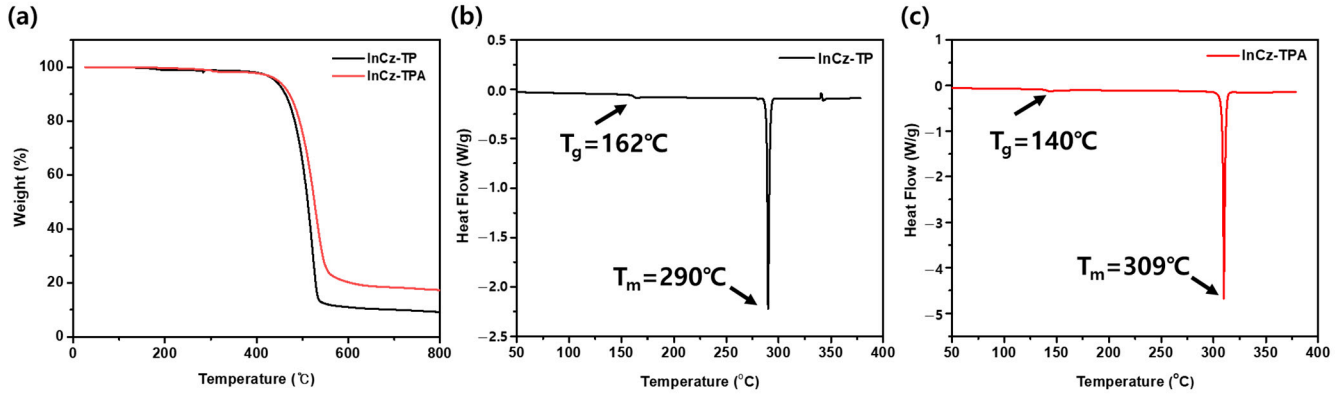

Figure 4. (**a**) TGA and (**b**,**c**) DSC curves for InCz-TP and InCz-TPA.

3.5. Electroluminescence Properties

To evaluate the electroluminescent (EL) capabilities of the newly synthesized InCz-TP and InCz-TPA, red phosphorescent OLEDs were constructed using them as hosts. The device architecture was optimized with the following configuration: ITO/1,4,5,8,9,11-hexaazatriphenylenehexacarbonitrile (HAT-CN) (10 nm)/1,1-bis[(di-4-tolylamino)phenyl]cyclohexane (TAPC) (30 nm)/tris(4-carbazoyl-9-ylphenyl)amine (TCTA) (10 nm)/host: 10 wt% bis(1-phenylisoquinoline)(acetylacetonate)iridium(III) ($Ir(piq)_2(acac)$) (20 nm)/1,3,5-tris(3-pyridyl-3-phenyl)benzene (TmPyPb) (30 nm)/LiF (1 nm)/Al (200 nm). In this configuration, HAT-CN functioned as the hole injection layer (HIL), TAPC as the HTL, TCTA as the exciton blocking layer (EBL), and TmPyPb as both the electron-transporting layer (ETL) and hole-blocking layer (HBL), whereas LiF and Al served as the electron injection layer and cathode, respectively.

The T_1 values of InCz-TP and InCz-TPA were determined from 77 K PL spectra as 2.81 eV and 2.78 eV, respectively, based on the spectral onset (Figure S12). Both materials exhibit high T_1 levels, making them suitable hosts for blue, green, and red phosphorescent dopants. In this study, the red phosphorescent dopant $Ir(piq)_2(acac)$, which has a T_1 level of 1.98 eV, was first employed, as efficient energy transfer from the host to the dopant is anticipated (Figure S13) [31,32]. The application of blue and green phosphorescent dopants will be explored in future work. The comprehensive EL data are presented in Figure 5 and Table 2. Under a constant current density of 10 mA/cm^2, driving voltages of 4.63 V for the InCz-TP-based device and 5.39 V for the InCz-TPA-based device were recorded. The observed voltage increase of 0.76 V for InCz-TPA is primarily linked to its shallower LUMO level (−2.26 eV) relative to InCz-TP (−2.34 eV), which effectively elevates the injection barrier for electrons originating from the ETL (Figure S14). Nevertheless, InCz-TPA demonstrated superior overall efficiency performance, with both its

current (CE) and power (PE) efficiencies outperforming those of InCz-TP due to its better emission efficiency (Figure S15). Most notably, the maximum EQE for the InCz-TPA-based device reached 8.50%, compared to 6.23% for InCz-TP, representing a performance boost of approximately 36%. This efficiency enhancement is ascribed to the TPA moiety, which facilitates more vigorous radiative recombination and supports robust energy transfer to the guest molecules. The CE and EQE of InCz-TPA at 10 mA/cm^2 were measured to be 5.5 cd/A and 7.5%, respectively. These results are at a similar level to those reported for devices based on the commonly used mCBP host, which exhibit a CE of 5.5 cd/A and an EQE of 7.8% [33]. However, further improvements in device performance are expected through optimization, such as employing different HTL and ETL materials or adjusting the layer thickness. Both devices yielded nearly identical CIE coordinates of (0.678, 0.317) and (0.680, 0.318), with a consistent EL emission peak at 628 nm, thereby confirming stable dopant emission in both cases.

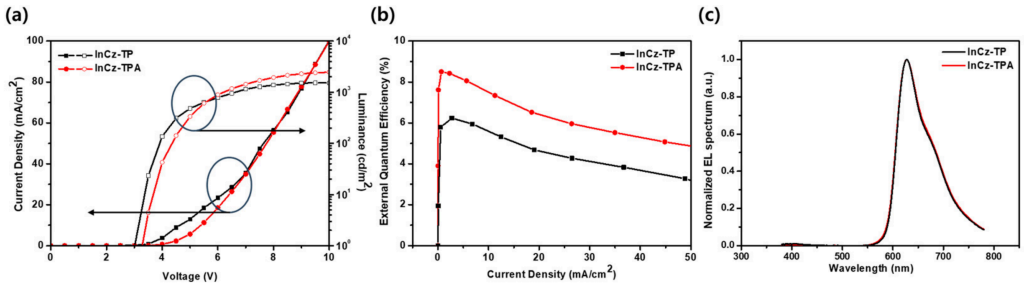

Figure 5. EL performance of doped OLED devices: (**a**) current density (J)–voltage (V)–luminance (L) characteristics, (**b**) EQE vs. J curves, and (**c**) EL spectra.

Table 2. EL performance of doped devices.

	Voltage [a] (V)	CE_{max} (cd/A)	PE_{max} (lm/W)	EQE_{max} (%)	CIE [a] (x, y)	EL_{max} [b] (nm)
InCz-TP	4.63	4.59	3.81	6.23	(0.678, 0.317)	628
InCz-TPA	5.39	6.23	4.95	8.50	(0.680, 0.318)	628

[a] Operating voltage measured at 10 mA/cm^2, [b] Measured at 5 V.

4. Conclusions

In this study, two novel red host materials, InCz-TP and InCz-TPA, were synthesized by introducing bulky TP and TPA substituents into an InCz core, which exhibits strong electron-donating ability, high photoluminescence quantum yield, and excellent thermal stability. InCz-TPA showed a higher PLQY than InCz-TP due to the strong electron-donating effect of the TPA group, and theoretical calculations revealed a dominant LE state along with a high oscillator strength. Both materials exhibited decomposition temperatures exceeding 440 °C, ensuring sufficient thermal stability during device operation. Devices using Ir(piq)$_2$(acac) as the dopant and InCz-TPA as the host demonstrated superior EL performance compared to those based on InCz-TP, achieving a maximum EQE of 8.50%. This improvement can be explained by the role of the TPA substituent in facilitating radiative decay and enabling efficient energy transfer to the dopant. Based on these findings, introducing appropriately designed electron-donating moieties into the indolocarbazole framework is expected to enable the development of highly efficient red phosphorescent OLEDs.

Supplementary Materials: The following supporting information can be downloaded from https://www.mdpi.com/article/10.3390/app16104713/s1: Figure S1: ^{1}H-NMR spectrum of compound (1);

Figure S2: ^{1}H-NMR spectrum of compound (2); Figure S3: ^{1}H-NMR spectrum of InCz, compound (3); Figure S4: ^{13}C-NMR spectrum of InCz, compound (3); Figure S5: ^{1}H-NMR spectrum of compound (4); Figure S6: ^{1}H-NMR spectrum of compound (5); Figure S7: ^{1}H-NMR spectrum of InCz-TP; Figure S8: ^{13}C-NMR spectrum of InCz-TP; Figure S9: ^{1}H-NMR spectrum of InCz-TPA; Figure S10: ^{13}C-NMR spectrum of InCz-TPA; Figure S11: TRPL curve of InCz-TP and InCz-TPA (IRF: instrument response function); Figure S12: PL spectra of InCz-TP and InCz-TPA at 77K; Figure S13: Schematic illustration of energy levels (S_1, T_1, S_0) and energy transfer processes in host–dopant systems; Figure S14: Band diagram of OLED doping device; Figure S15: EL performance of doped OLED devices: (a) CE vs. J curves and (b) PE vs. J curves.

Author Contributions: Conceptualization, M.G., C.L. (Changjun Lee) and J.P.; methodology, M.G.; validation, M.G., C.L. (Changmin Lee) and S.P.; formal analysis, S.O. and K.L.; investigation, C.L. (Changjun Lee) and H.L.; resources, J.P.; writing—original draft preparation, M.G., C.L. (Changjun Lee) and H.L.; writing—review and editing, H.L. and J.P.; visualization, M.G., C.L. (Changmin Lee), S.P., K.L. and H.L.; supervision, J.P.; project administration, J.P.; funding acquisition, J.P. All authors have read and agreed to the published version of the manuscript.

Funding: This research was supported by Basic Science Research Program through the National Research Foundation of Korea (NRF) funded by the Ministry of Education (RS-2020-NR049601). This work was partly supported by the GRRC program of Gyeonggi province [(GRRCKYUNGHEE2023-B01), Development of ultra-fine process materials based on the sub-nanometer class for the next-generation semiconductors]. This work was supported by the Technology Innovation Program (RS-2024-00423271, Development of mass production technology for high-quality perovskite light-emitting nanocrystal) funded by the Ministry of Trade, Industry & Energy (MOTIE, Republic of Korea). This work was supported by the Technology Innovation Program (RS-2024-00419747, Development of Materials and Devices Based on Tandem Device to Achieve High Efficiency and Long Lifetime Blue OLEDs for IT Display Applications) funded By the Ministry of Trade, Industry & Energy (MOTIE, Republic of Korea). This research was supported by Global–Learning & Academic research institution for Master's and PhD students and Postdocs (G-LAMP) Program of the National Research Foundation of Korea (NRF) grant funded by the Ministry of Education (No. RS-2025-25442355).

Institutional Review Board Statement: Not applicable.

Informed Consent Statement: Not applicable.

Data Availability Statement: The original contributions presented in this study are included in the article/Supplementary Materials. Further inquiries can be directed to the corresponding author.

Conflicts of Interest: The authors declare no conflicts of interest.

References

1. Wei, Q.; Fei, N.; Islam, A.; Lei, T.; Hong, L.; Peng, R.; Fan, X.; Chen, L.; Gao, P.; Ge, Z. Small-Molecule Emitters with High Quantum Efficiency: Mechanisms, Structures, and Applications in OLED Devices. *Adv. Opt. Mater.* **2018**, *6*, 1800512. [CrossRef]
2. Kang, S.W.; Baek, D.-H.; Ju, B.-K.; Park, Y.W. Green Phosphorescent Organic Light-Emitting Diode Exhibiting Highest External Quantum Efficiency with Ultra-Thin Undoped Emission Layer. *Sci. Rep.* **2021**, *11*, 8436. [CrossRef]
3. Diesing, S.; Zhang, L.; Zysman-Colman, E.; Samuel, I.D.W. A Figure of Merit for Efficiency Roll-Off in TADF-Based Organic LEDs. *Nature* **2024**, *627*, 747–753. [CrossRef]
4. van der Zee, B.; Li, Y.; Wetzelaer, G.-J.A.H.; Blom, P.W.M. Triplet-Polaron-Annihilation-Induced Degradation of Organic Light-Emitting Diodes Based on Thermally Activated Delayed Fluorescence. *Phys. Rev. Appl.* **2022**, *18*, 064002. [CrossRef]
5. Baldo, M.A.; O'Brien, D.F.; You, Y.; Shoustikov, A.; Sibley, S.; Thompson, M.E.; Forrest, S.R. Highly Efficient Phosphorescent Emission from Organic Electroluminescent Devices. *Nature* **1998**, *395*, 151–154. [CrossRef]
6. Uoyama, H.; Goushi, K.; Shizu, K.; Nomura, H.; Adachi, C. Highly Efficient Organic Light-Emitting Diodes from Delayed Fluorescence. *Nature* **2012**, *492*, 234–238. [CrossRef]
7. Kwon, N.Y.; Park, S.H.; Koh, C.W.; Park, J.Y.; Kang, M.J.; Baek, H.I.; Youn, J.; Park, S.; Han, C.W.; Cho, M.J.; et al. Rational Molecular Design Strategy for Host Materials in Thermally Activated Delayed Fluorescence-OLEDs Suitable for Solution Processing. *ACS Appl. Mater. Interfaces* **2023**, *15*, 28277–28287. [CrossRef]

8. Yuan, W.; Huang, T.; Zhou, J.; Tang, M.-C.; Zhang, D.; Duan, L. High-Efficiency and Long-Lifetime Deep-Blue Phosphorescent OLEDs Using Deuterated Exciplex-Forming Host. *Nat. Commun.* **2025**, *16*, 4446. [CrossRef]
9. Gnanasekaran, P.; Chen, Y.-T.; Tseng, Y.-T.; Su, K.-Y.; Lin, Y.-T.; Yiu, T.C.; Chang, C.-H.; Chang, Y.J. Perceiving the Influence of Phenyl-Carbazole Isomers on Sulfone/Thioxanthone-Based D–A–D Hosts: Realizing Efficient Red-Phosphorescent OLEDs. *J. Mater. Chem. C* **2024**, *12*, 2203–2215. [CrossRef]
10. Meng, Z.; Zhu, Y.; Li, H.; Zhang, X.; Shang, Y.; Kuang, C.; Meng, H. Highly Efficient and Stable Pure-Red Phosphorescent Organic Light-Emitting Diodes Based on Heptacyclic Bipolar Hosts Featuring an Armor-Like Structure. *J. Mater. Chem. C* **2024**, *12*, 9993–9998. [CrossRef]
11. Yang, S.; Guan, D.; Yang, M.; Tian, J.; Chu, W.; Sun, Z. Synthesis and Characterization of Novel Butterfly-Shaped Aryl-Substituted Indolo[2,3-a]carbazole Derivatives. *Tetrahedron Lett.* **2015**, *56*, 2223–2227. [CrossRef]
12. Braveentha, R.; Bae, I.-J.; Raagulan, K.; Kim, S.; Kim, S.; Kim, M.; Chai, K.Y. Dibenzothiophene-Indolocarbazole-Based Bipolar Material: Host for Green Phosphorescent OLEDs and Non-Doped Fluorescent Emitter. *Dye. Pigm.* **2019**, *162*, 466–474. [CrossRef]
13. Huh, D.H.; Kim, G.W.; Kim, G.H.; Kulshreshtha, C.; Kwon, J.H. High Hole Mobility Hole Transport Material for Organic Light-Emitting Devices. *Synth. Met.* **2013**, *180*, 79–84. [CrossRef]
14. Zheng, X.; Cao, F.; Wang, C.; Tsuboi, T.; Zhu, Y.; Ai, Q.; Deng, C.; Wang, D.; Su, L.; Liu, Z.; et al. Expanding the hole delocalization range in excited molecules for stable organic light-emitting diodes employing thermally activated delayed fluorescence. *J. Mater. Chem. C* **2020**, *8*, 10021–10030. [CrossRef]
15. Lee, H.J.; Lee, H.L.; Han, S.H.; Lee, J.Y. Novel secondary acceptor based molecular design for superb lifetime in thermally activated delayed fluorescent organic light-emitting diodes through high bond energy and fast up-conversion. *Chem. Eng. J.* **2022**, *427*, 130988. [CrossRef]
16. Yang, H.; Li, Y.; Zhao, Y.; Yu, S.; Ma, H.; Qian, L.; Wang, R.; Yu, T.; Su, W. Four New Bipolar Indolo[3,2-b]carbazole Derivatives for Blue OLEDs. *Dye. Pigm* **2021**, *187*, 109096. [CrossRef]
17. Kumar, K.; Thakur, D.; Karmakar, A.; Patra, S.; Kumar, A.; Banik, S.; Ghosh, S. Indolo[3,2-a]carbazoles as Engineered Materials for Optoelectronic Applications: Synthesis, Structural Insights, and Computational Screening. *J. Org. Chem.* **2024**, *89*, 7394–7407. [CrossRef]
18. Kautny, P.; Wu, Z.; Eichelter, J.; Horkel, E.; Stöger, B.; Chen, J.; Ma, D.; Fröhlich, J.; Lumpi, D. Indolo[3,2,1-jk]carbazole based planarized CBP derivatives as host materials for PhOLEDs with low efficiency roll-off. *Org. Electron.* **2016**, *34*, 237–245. [CrossRef]
19. Oner, S.; Bryce, M.R. A review of fused-ring carbazole derivatives as emitter and/or host materials in organic light emitting diode (OLED) applications. *Mater. Chem. Front.* **2023**, *7*, 4304–4338. [CrossRef]
20. Shin, E.; Sung, B.; Joo, C.W.; Kim, D.; Kim, J.; Lee, J.; Kim, Y.H. Novel indolocarbazole-based bipolar host materials for fabri-cating green phosphorescent organic light-emitting diodes with high efficiency and low roll-off. *Dye. Pigm.* **2024**, *226*, 112147. [CrossRef]
21. Zhang, Y.; Chen, F.; Zheng, J.; Song, Z.; Wang, Y.; Mao, Y.; Tang, J.; Guo, J.; Wang, X. Aggregate Emission Behaviors and Reversible Mechanofluorochromic Properties of α-Cyanostilbene Functionalized Indolo[3,2-b]carbazole Derivatives. *CrystEngComm* **2022**, *24*, 7405–7411. [CrossRef]
22. Wang, J.; Zhang, J.; Jiang, C.; Yao, C.; Xi, X. Effective Design Strategy for Aggregation-Induced Emission and Thermally Activated Delayed Fluorescence Emitters Achieving 18% External Quantum Efficiency Pure-Blue OLEDs with Extremely Low Roll-Off. *ACS Appl. Mater. Interfaces* **2021**, *13*, 57713–57724. [CrossRef]
23. Park, S.; Kwon, H.; Park, S.; Oh, S.; Lee, K.; Lee, H.; Kang, S.; Park, D.; Park, J. New Bipolar Host Materials Based on Indolocarbazole for Red Phosphorescent OLEDs. *Materials* **2024**, *17*, 4347. [CrossRef]
24. Kim, Y.; Ham, Y.; Le, T.N.; Yang, H.; Lee, J.; Suh, M.C. Boosting Hole Mobility: Indenofluorene-Arylamine Copolymers and Their Impact on Solution-Processed OLED Performance. *ACS Appl. Mater. Interfaces* **2024**, *16*, 31372–31383. [CrossRef]
25. Kumar, K.; Kesavan, K.K.; Kumar, S.; Chen, F.R.; Karmakar, A.; Jayakumar, J.; Goswami, R.; Banik, S.; Jou, J.H.; Ghosh, S. Computational Evaluation with Experimental Validation: Arylamine-Based Functional Hole-Transport Materials for Energy-Efficient Solution-Processed OLEDs. *J. Phys. Chem. C* **2023**, *127*, 18560–18573. [CrossRef]
26. Neese, F.; Wennmohs, F.; Becker, U.; Riplinger, C. The ORCA Quantum Chemistry Program Package. *J. Chem. Phys.* **2020**, *152*, 224108. [CrossRef]
27. Li, W.J.; Liu, D.D.; Shen, F.Z.; Ma, D.G.; Wang, Z.M.; Feng, T.; Xu, Y.X.; Yang, B.; Ma, Y.G. A Twisting Donor–Acceptor Molecule with an Intercrossed Excited State for Highly Efficient, Deep-Blue Electroluminescence. *Adv. Funct. Mater.* **2012**, *22*, 2797–2803. [CrossRef]
28. Gorse, A.D.; Pesquer, M. Intramolecular Charge Transfer Excited State Relaxation Processes in Para-Substituted N,N-Dimethylaniline: A Theoretical Study Including Solvent Effects. *J. Phys. Chem.* **1995**, *99*, 4039–4049. [CrossRef]
29. Lim, H.; Cheon, H.J.; Woo, S.-J.; Kwon, S.-K.; Kim, Y.-H.; Kim, J.-J. Highly Efficient Deep-Blue OLEDs using a TADF Emitter with a Narrow Emission Spectrum and High Horizontal Emitting Dipole Ratio. *Adv. Mater.* **2020**, *32*, 2004083. [CrossRef]

30. Braveenth, R.; Lee, H.; Park, J.D.; Yang, K.J.; Hwang, S.J.; Naveen, K.R.; Lampande, R.; Kwon, J.H. Achieving Narrow FWHM and High EQE over 38% in Blue OLEDs Using Rigid Heteroatom-Based Deep Blue TADF Sensitized Host. *Adv. Funct. Mater.* **2021**, *31*, 2105805. [CrossRef]
31. Wang, Y.; Yun, J.H.; Wang, L.; Lee, J.Y. High Triplet Energy Hosts for Blue Organic Light-Emitting Diodes. *Adv. Funct. Mater.* **2021**, *31*, 2008332. [CrossRef]
32. Zhang, Y.; Zhang, D.; Huang, T.; Zhang, Q.; Zhao, C.; Duan, L. High-Efficiency Deep-Red Phosphorescent Organic Light-Emitting Diodes with External Quantum Efficiencies of over 30% via Synergistic Energy Transfer. *Sci. Adv.* **2022**, *8*, eabp9203.
33. Kwon, H.; Kang, S.; Park, S.; Oh, S.; Kim, S.-T.; Lee, K.; Lee, H.; Park, J. Selenium-Containing Multi-Resonance Thermally Activated Delayed Fluorescence Host Material for Green and Red Phosphorescent OLEDs. *Materials* **2025**, *18*, 2040. [CrossRef] [PubMed]

Disclaimer/Publisher's Note: The statements, opinions and data contained in all publications are solely those of the individual author(s) and contributor(s) and not of MDPI and/or the editor(s). MDPI and/or the editor(s) disclaim responsibility for any injury to people or property resulting from any ideas, methods, instructions or products referred to in the content.